JOURNAL OF AIRCRAFT
Vol. 38, No. 5, September–October 2001

Parametric Study of Transient Spoiler Aerodynamics with Two-Equation Turbulence Models

Seong-Wook Choi*
Korea Aerospace Research Institute, Taejon 305-333, Republic of Korea
Keun-Shik Chang†
Korea Advanced Institute of Science and Technology, Taejon 305-701, Republic of Korea
and
Honam Ok*
Korea Aerospace Research Institute, Taejon 305-333, Republic of Korea

The transient response of an airfoil to a rapidly deploying spoiler is numerically investigated using the turbulent compressible Navier–Stokes equations in two dimensions. The algebraic Baldwin–Lomax model, Wilcox k–ω model, and shear stress transport k–ω turbulence models were used to calculate the unsteady separated flow due to the rapid spoiler deployment. The spoiler motion relative to a stationary airfoil is treated using an overset grid bounded by a dynamic domain-dividing line, which has been devised by the authors. The adverse effects of the spoiler influenced by the spoiler location and the hinge gap are expounded. The numerical results are in reasonably good agreement with the existing experimental data.

Introduction

A SPOILER deployed on the upper surface of a wing is normally actuated in a very short time. It forces the flow to separate with a resultant loss of lift and an increase of drag. The spoiler has a variety of current and potential uses as a control device for aircraft.[1] For instance, active flow control technology (AFC) has received much attention due to the capability of relaxed stability, suppression of flutter, and reduction of vibration levels.[2] However, there is a strong adverse aerodynamic effect in the initial stage of the spoiler deployment. Its strength depends not only on the flight conditions such as angle of attack and flight speed but also on the spoiler deploying rate and spoiler location. The time delay due to the adverse lift can pose considerable difficulty in the design of a proper feedback control system.[3] To reduce this adverse effect, various spoiler/hinge gap configurations have been proposed.[1] The adverse lift, on the other hand, can be useful if it were utilized as a dynamic lift for the AFC.[4] An example is gust alleviation through periodic deploying and retraction of the spoiler.[4]

Only a few experimental studies have been conducted on the rapidly deploying spoiler. Mabey[2] advises that time delay and adverse lift of a spoiler should be expressed as a function of nondimensional deploying time Ut/c. Consigny et al.[3] concluded that significant amount of adverse lift and time delay can result from the spoiler even at a moderate rate of rotation. Yeung et al.[5] have shown that the adverse lift can be reduced using a base-vented spoiler in which the spoiler vortex is alleviated by the counterrotating vortex generated by the through flow.

A numerical study on the rapidly deploying spoiler was conducted by Xu and Yeung,[6] who used the combined panel and discrete vortex method to simulate the base venting experimentally investigated earlier.[5] Recently, the present authors[7] conducted Navier–Stokes flow computation on the rapidly deploying spoiler using the Baldwin–Lomax turbulence model.[8] They[7] investigated the genesis and the mechanism for the generation of the adverse lift as a function of the deploying rate of the spoiler.

In the present computational study, the k–ω turbulence model, the Wilcox k–ω, model and the shear stress transport (SST) k–ω model, are considered additionally to the algebraic Baldwin–Lomax model[8] to demonstrate the improved accuracy. The result from the experimental study by Yeung et al.[5] are numerically reproduced. The two significant features of the spoiler, the adverse lift and the time delay, are analyzed parametrically in terms of the spoiler location and the hinge gap size for base venting.

Governing Equations

The two-dimensional unsteady compressible Navier–Stokes equations can be written in an integral form on a moving grid system. For an arbitrary grid cell Ω with its boundary $\partial\Omega$, they are

$$\frac{\partial}{\partial t}\iint_{\Omega} \boldsymbol{Q}\,\mathrm{d}V + \int_{\partial\Omega} \boldsymbol{F}(\boldsymbol{Q})\cdot\boldsymbol{n}\,\mathrm{d}S = \int_{\partial\Omega} \boldsymbol{G}(\boldsymbol{Q})\cdot\boldsymbol{n}\,\mathrm{d}S \tag{1}$$

where V is the cell volume, $\boldsymbol{Q}$ is the conservative variable vector, and $\boldsymbol{F}(\boldsymbol{Q})$ is the inviscid flux vector represented by

$$\boldsymbol{Q} = \begin{bmatrix} \rho \\ \rho u \\ \rho v \\ e \end{bmatrix}, \qquad \boldsymbol{F}(\boldsymbol{Q})\cdot\boldsymbol{n} = \begin{bmatrix} \rho\bar{U} \\ \rho u\bar{U} + pn_x \\ \rho v\bar{U} + pn_y \\ (e+p)\bar{U} + pU_{gn} \end{bmatrix} \tag{2}$$

where n_x and n_y are the Cartesian components of the surface unit vector $\boldsymbol{n}$ normal to the boundary $\partial\Omega$ and u and v are velocity components of $\boldsymbol{U}$ in the x and y directions, respectively. $\bar{U}$ is the normal component of the relative velocity, defined by $\bar{U} = \boldsymbol{n}\cdot(\boldsymbol{U}-\boldsymbol{U}_g) = U_n - U_{gn}$, where $\boldsymbol{U}_g$ is the grid velocity. The variables ρ and e are density and total internal energy per unit volume, respectively. The viscous flux vector is

$$\boldsymbol{G}(\boldsymbol{Q})\cdot\boldsymbol{n} = \frac{M_\infty}{Re}\begin{bmatrix} 0 \\ \tau_{xx}n_x + \tau_{yx}n_y \\ \tau_{xy}n_x + \tau_{yy}n_y \\ (u\tau_{xx} + v\tau_{xy} - q_x)n_x + (u\tau_{yx} + v\tau_{yy} - q_y)n_y \end{bmatrix} \tag{3}$$

Received 14 June 2000; presented as Paper 2001-0864 at the AIAA 39th Aerospace Sciences Meeting and Exhibit; Reno, NV, 8–11 January, 2001; revision received 20 March 2001; accepted for publication 22 April 2001.

*Senior Researcher, Aerodynamics Department. Member AIAA.
†Professor, Department of Aerospace Engineering. Member AIAA.

The shear stress τ and heat flux q are written in tensor form as

$$\tau_{ij} = (\mu + \mu_t)\left(\frac{\partial u_i}{\partial x_j} + \frac{\partial u_j}{\partial x_i} - \frac{2}{3}\frac{\partial u_k}{\partial x_k}\delta_{ij}\right)$$

and

$$q_i = -\frac{1}{\gamma - 1}\left(\frac{\mu}{Pr} + \frac{\mu_t}{Pr_t}\right)\frac{\partial T}{\partial x_i}$$

The Prandtl number Pr is taken for air as 0.72, and the turbulent Prandtl number Pr_t is 0.9. The laminar coefficient of viscosity, μ, is described by Sutherland's law.

Numerical Method

The basic solution algorithm for the Navier–Stokes equations (1) is the second-order fully implicit scheme with a subiterative time stepping procedure.[9] In delta form, we have

$$\left[I\frac{V}{\Delta t} + \frac{\vartheta}{1+\varphi}\left(\frac{\partial \boldsymbol{R}}{\partial \boldsymbol{Q}}\right)\right](\boldsymbol{Q}^{p+1} - \boldsymbol{Q}^p) = -\frac{1}{1+\varphi}\boldsymbol{R}(\boldsymbol{Q}^p) - \frac{V}{\Delta t}\left[\boldsymbol{Q}^p - \frac{1+2\varphi}{1+\varphi}\boldsymbol{Q}^n + \frac{\varphi}{1+\varphi}\boldsymbol{Q}^{n-1}\right] \tag{4}$$

where $\boldsymbol{R}(\boldsymbol{Q})$ is the residual vector obtained by summing up the inviscid and viscous fluxes on the four faces of a cell. In Eq. (4), the n and $n-1$ terms are evaluated from previous time levels, and after iterating p times the solution at time level $n+1$ will be taken from the most recent $\boldsymbol{Q}^{p+1}$. The parameters ϑ and φ avail choice of different schemes: first- and second-order implicit schemes.

We solve Eq. (4) using the point symmetric-Gauss–Seidel (SGS) relaxation scheme (see Ref. 10). The inviscid flux terms are computed using Roe's flux difference splitting upwind method; second-order spatial accuracy is obtained by the MUSCL approach using the flux limiter of Venkatakrishnan.[11] The viscous flux across each cell face is determined by averaging of the two cell center values of the adjacent cells. Equation (4) can be applied to an overset grid system by simply inserting the hole-point flag $\boldsymbol{i}_b$ into the equations. The solution $\boldsymbol{Q}^{n+1}$, obtained on one of the overset grid systems, is interpolated bilinearly to assign boundary values on the other grid system. During the point SGS relaxation procedure, data transfer for the variable $\Delta\boldsymbol{Q}$ is also performed by the bilinear interpolation made both ways. Using this approach, it was possible to elevate the Courant–Friedrichs–Lewy (CFL) number up to the level of a single grid (see Ref. 7).

Turbulence Modeling

In this study, the algebraic Baldwin–Lomax[8] turbulence model and two k–ω models are used. Although there are some modified versions of the Baldwin–Lomax model (see Refs. 12 and 13), the original model[8] is used in the present study. The most popular nonalgebraic turbulence models for engineering applications are the two-equation eddy viscosity models such as the k–ε and k–ω models.[14] These models have, however, shortcomings: lack of sensitivity to the strong adverse pressure gradient and dependency on the freestream.[14,15] To overcome these deficiencies, the baseline (BSL) k–ω model has been developed in Ref. 15 by combining the k–ε and k–ω models. The BSL k–ω model was further modified to the SST k–ω model[15] to improve flow sensitivity to the strong adverse pressure gradient. The nondimensional BSL k–ω equations are written in integral form as

$$\frac{\partial}{\partial t}\iiint_\Omega \boldsymbol{Q}_T\,\mathrm{d}V + \int_{\partial\Omega}\boldsymbol{F}_T(\boldsymbol{Q}_T)\cdot\boldsymbol{n}\,\mathrm{d}S = \int_{\partial\Omega}\boldsymbol{G}_T(\boldsymbol{Q}_T)\cdot\boldsymbol{n}\,\mathrm{d}S + \iiint_\Omega \boldsymbol{S}_T(\boldsymbol{Q}_T)\,\mathrm{d}V \tag{5}$$

where $\boldsymbol{Q}_T$ is the conservative variable vector for k and ω and $\boldsymbol{F}_T(\boldsymbol{Q}_T)$ is the flux vector:

$$\boldsymbol{Q}_T = \begin{bmatrix}\rho k\\ \rho\omega\end{bmatrix}, \qquad \boldsymbol{F}_T(\boldsymbol{Q}_T)\cdot\boldsymbol{n} = \begin{bmatrix}\rho k\bar{U}\\ \rho\omega\bar{U}\end{bmatrix} \tag{6}$$

The diffusion terms $\boldsymbol{G}_T(\boldsymbol{Q}_T)$ are represented by

$$\boldsymbol{G}_T(\boldsymbol{Q}_T)\cdot\boldsymbol{n} = \frac{M_\infty}{Re}\begin{bmatrix}(\mu+\sigma_k\mu_t)\left(n_x\dfrac{\partial k}{\partial x} + n_y\dfrac{\partial k}{\partial y}\right)\\ (\mu+\sigma_\omega\mu_t)\left(n_x\dfrac{\partial \omega}{\partial x} + n_y\dfrac{\partial \omega}{\partial y}\right)\end{bmatrix} \tag{7}$$

The source terms $\boldsymbol{S}_T(\boldsymbol{Q}_T)$ consist of production and destruction terms,

$$\boldsymbol{S}_T(\boldsymbol{Q}_T) = \begin{bmatrix}\tau_{ij}\dfrac{\partial u_i}{\partial x_j}\left(\dfrac{M_\infty}{Re}\right) - \beta^*\rho\omega k\left(\dfrac{Re}{M_\infty}\right)\\ \dfrac{\gamma}{v_t}\tau_{ij}\dfrac{\partial u_i}{\partial x_j}\left(\dfrac{M_\infty}{Re}\right) - \beta\rho\omega^2 k\left(\dfrac{Re}{M_\infty}\right) + 2(1-F_1)\rho\sigma_{\omega 2}\dfrac{1}{\omega}\dfrac{\partial k}{\partial x_j}\dfrac{\partial \omega}{\partial x_j}\left(\dfrac{M_\infty}{Re}\right)\end{bmatrix} \tag{8}$$

The turbulent shear stress terms are, in tensor form,

$$\tau_{ij} = \mu_t\left(\frac{\partial u_i}{\partial x_j} + \frac{\partial u_j}{\partial x_i} - \frac{2}{3}\frac{\partial u_k}{\partial x_k}\delta_{ij}\right) - \frac{2}{3}\rho k\delta_{ij}\left(\frac{Re}{M_\infty}\right)$$

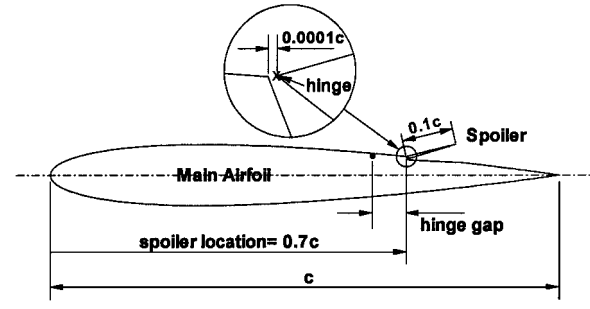

Fig. 1 Spoiler on the NACA 0012 airfoil.

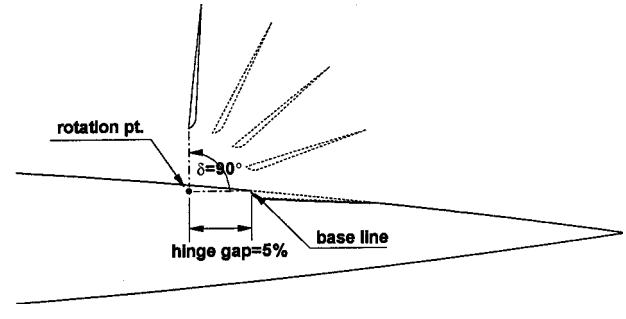

Fig. 2 Rotation of the spoiler with a 5% hinge gap.

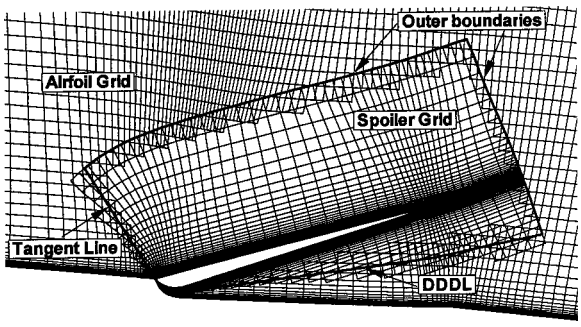

Fig. 3 Grid around airfoil and spoiler at an instant; hole-cutting boundary shown.

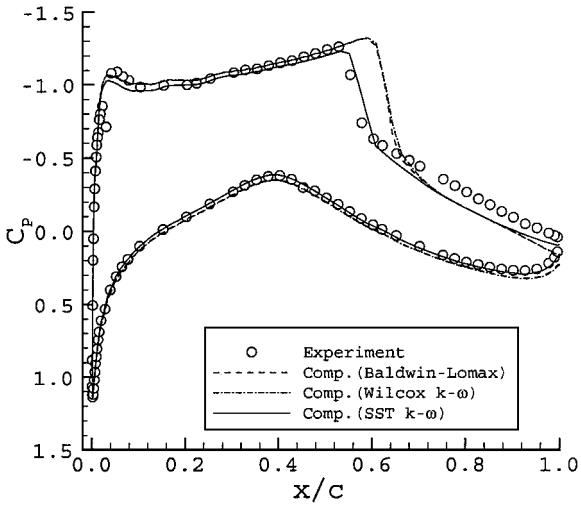

Fig. 4 Surface pressure coefficient of the RAE 2822 airfoil (case 10: $M_\infty = 0.75$, $\alpha = 2.81$ deg, $Re = 6.2 \times 10^6$).

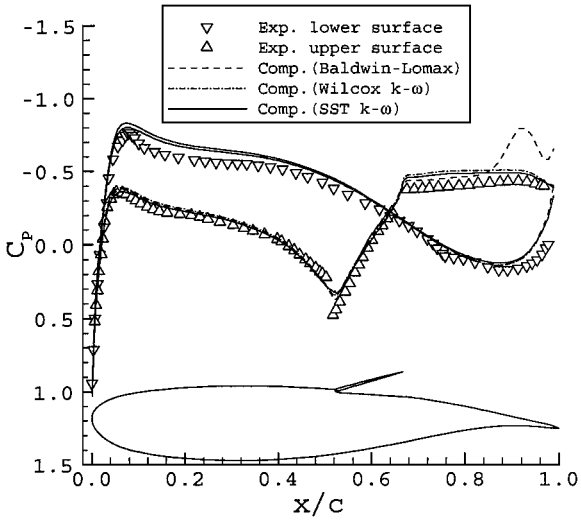

a) Time-averaged surface pressure coefficient

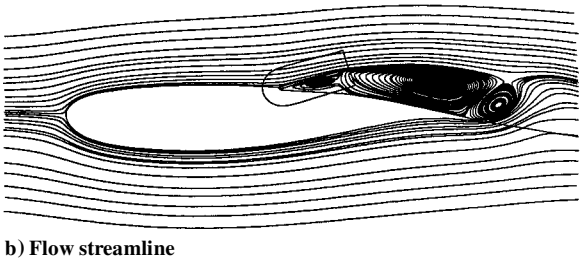

b) Flow streamline

Fig. 5 RA16SC airfoil with the spoiler stationary at $\delta = 20$ deg, ($M_\infty = 0.3$, $\alpha = 0$ deg, $Re = 1.9 \times 10^6$).

The constants in the BSL and SST models, for example, ϕ, are determined by blending the constants in the Wilcox k–ω model, for example, ϕ_1, and those in the standard k–ε model, for example ϕ_2, by setting $\phi = F_1\phi_1 + (1 - F_1)\phi_2$, where F_1 is a blend function (see Ref. 15). The equations for the turbulence quantities are solved separately, that is, not coupled with the mean flow equations, using the same numerical procedure used for solving the mean flow equations (1).

Geometry and Grid

The NACA 0012 airfoil with a $0.1c$ spoiler located at $0.7c$ on the upper surface is shown in Fig. 1. From this BSL configuration, we will consider two more spoiler locations, namely, $0.5c$ and $0.3c$. Here, the hinge gap is defined as the distance, in percent, from the rotation center to the spoiler BSL. Figure 2 shows a spoiler deployed to 90 deg with a 5% hinge gap. The case of 0% hinge gap means that the rotation center is identical with the position of the leading edge of the spoiler. In our solutions, a very small gap ($0.0001c$) is allowed in the hinge (Fig. 1), to facilitate the use of an overset grid.[7]

The airfoil grid and the spoiler grid were first generated independently and then overlaid in a time-dependent manner by the algorithm of domain connectivity. The major airfoil grid and the minor spoiler grid have 301×65 and 101×41 C-type grids, respectively. The minimum grid spacing at the wall is $0.00002c$. Because an overset grid was used, we need to search for the hole points to exclude them from the flowfield computation and for the fringe points to avail data communication. With the geometry having a very small gap at the spoiler hinge and a very small initial clearance between the airfoil and the spoiler at zero deflection angle (necessary to

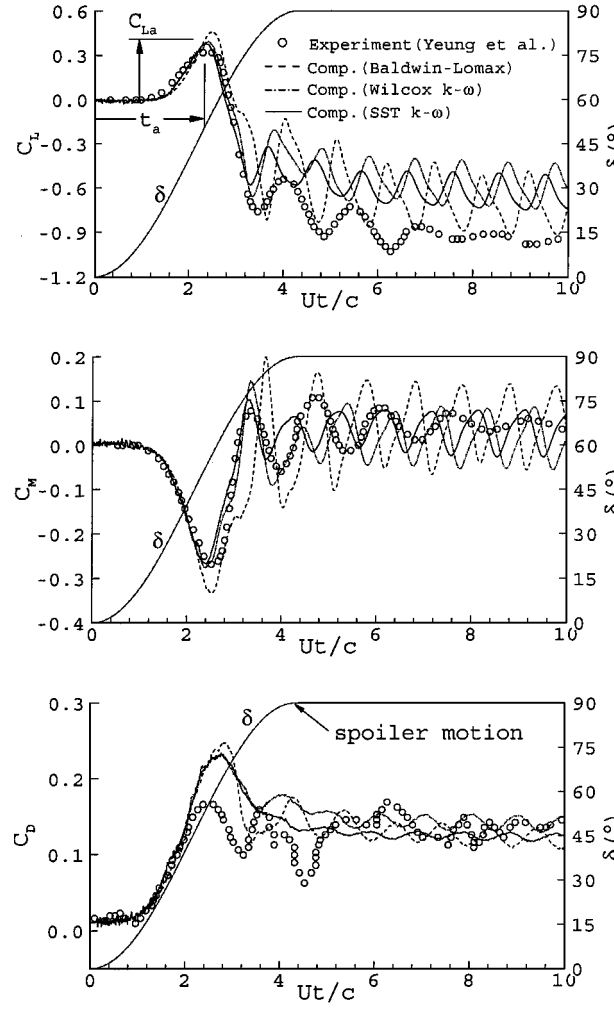

Fig. 6 Aerodynamic response to a rapidly deploying spoiler (ω = 620 deg/s).

prevent a vacuum state from being generated by the deployment of the spoiler), the conventional chimera grid would not be suitable because a hole-cutting boundary will have to be located at a distance inside the body. To overcome this difficulty, we devised a dynamic domain-dividing line (DDDL) for the hole-cutting boundary, which is made of a curve halving the distance between the airfoil and the spoiler plus a tangent line (Fig. 3). The tangent line is a straight line that is tangentially connected to the DDDL passing through the hinge gap. Joining the outer boundaries of the spoiler grid, the DDDL, and the tangent line at the intersection points, we have completely defined the hole-cutting boundary of the chimera grid system. Figure 3 shows both the airfoil grid and the spoiler grid generated this way. With rotation of the spoiler, DDDL and the tangent line of the spoiler grid system are regenerated at each time step, whereas the outer boundary is just under the solid body rotation.

Results and Discussion

Steady Flow Around an RAE 2822 Airfoil

Pressure predictions using three turbulence models are compared for the RAE 2822 (Ref. 16) airfoil in Fig. 4 for steady flow, case 10 ($M_\infty = 0.74$, $\alpha = 2.81$ deg, and $Re = 6.3 \times 10^6$), where flow separation is caused by shock/boundary-layer interaction. A C-type, 261×51 grid is used with 201 grid points on the airfoil surface. The flowfield is assumed fully turbulent with no consideration of flow transition. For steady flow, we used a CFL number of 10 and local time stepping. In Fig. 4, it is observed that the Baldwin–Lomax[8] and the Wilcox k–ω models give almost identical results, both overpredicting the strength of the shock with a more aft location. The SST k–ω model, in contrast, results in good overall agreement with the data, particularly for the shock position and the pressure distribution on the lower surface of the airfoil. The pressure on the upper surface downstream of the shock has some deviation.

Unsteady Flow Around a Stationary Spoiler

In this case, a 0.15c spoiler is hinged at the 0.52c position of the ONERA supercritical airfoil (RA16SC).[3] We consider subsonic flow with $M_\infty = 0.3$, $Re = 1.9 \times 10^6$, $\alpha = 0$ deg, and a spoiler angle $\delta = 20$ deg. Here, a time-accurate calculation is necessary because periodic vortex shedding is encountered. Figure 5 shows the computed surface pressure coefficients time averaged over a period and flow streamline resulted by the SST k–ω turbulence model. For the Baldwin–Lomax[8] turbulence model, a large discrepancy is evident near the trailing edge due to the vortex. A similar discrepancy has been found in other reports[17,18] using the Baldwin–Lomax turbulence model.[8] With the Wilcox k–ω and SST k–ω models, this discrepancy near the trailing edge has disappeared.

Rapidly Deploying Spoiler

We now calculate the adverse effects caused by a rapidly deploying spoiler. Here, the freestream velocity is 12 m/s ($M_\infty = 0.035$),

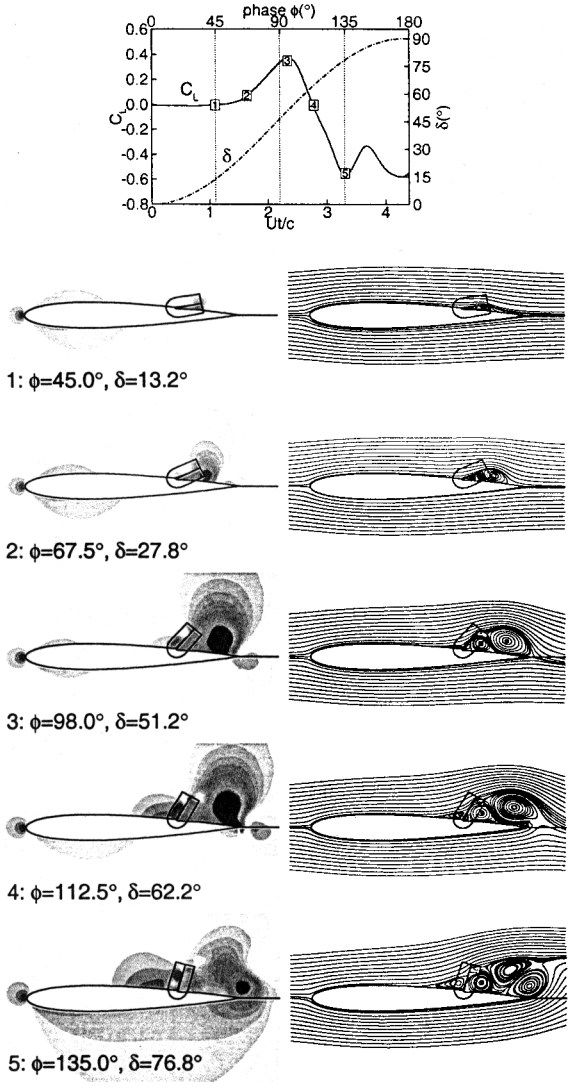

Fig. 7 Flow development with spoiler deployment (ω = 620 deg/s, spoiler location = 0.7c, hinge gap = 0%): left pressure distributions and right streamlines.

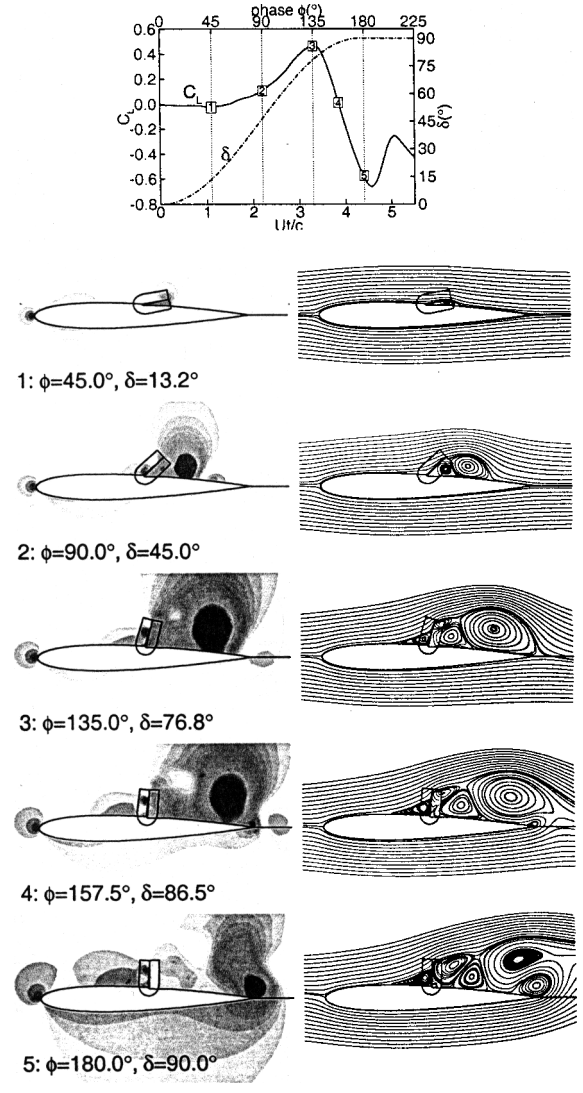

Fig. 8 Flow development with spoiler deployment (ω = 620 deg/s, spoiler location = 0.5c, hinge gap = 0%): left pressure distributions and right streamlines.

Reynolds number $= 3.5 \times 10^5$ based on the airfoil chord length, and the peak deployment angle of 90 deg are taken following the experiment of Yeung et al.[5] The spoiler has a ramp like motion given by

$$\delta(t) = \delta_0 + \tfrac{1}{2}(\delta_1 - \delta_0)\{1 - \cos[\pi(t - t_0)/(t_1 - t_0)]\} \qquad (9)$$

where $\delta_0 = 0$ deg, $\delta_1 = 90$ deg, and $t_0 = 0$. The constant t_1 is the deploying time set to 145 ms to yield a deployment rate of 620 deg/s. In this case, the spoiler hinge is at $0.7c$, and the hinge gap is zero. The unsteady calculation is started using the steady-state solution obtained for zero spoiler deflection angle. In this initial state, the maximum value of y^+ along the first grid points of the wall is 0.5.

The lift, pitching moment, and drag coefficients are compared in Fig. 6 with the experimental data. We define the adverse lift C_{La} as the maximum lift overshoot and the time delay t_a as the time up to the instant of maximum adverse lift. As seen, the adverse effect in the aerodynamic coefficients is well captured by all of the three turbulence models. However, the adverse lift and the time delay are somewhat overpredicted by the Baldwin–Lomax model[8] as compared with the experimental data. Best agreement is again seen for the SST k–ω model. After full deployment of the spoiler, the oscillatory lift coefficient decays to a steady state in the experiment, whereas the predictions indicate that a periodic oscillation with characteristic amplitude and frequency is sustained. Although the amplitudes and the mean values of the oscillations predicted by

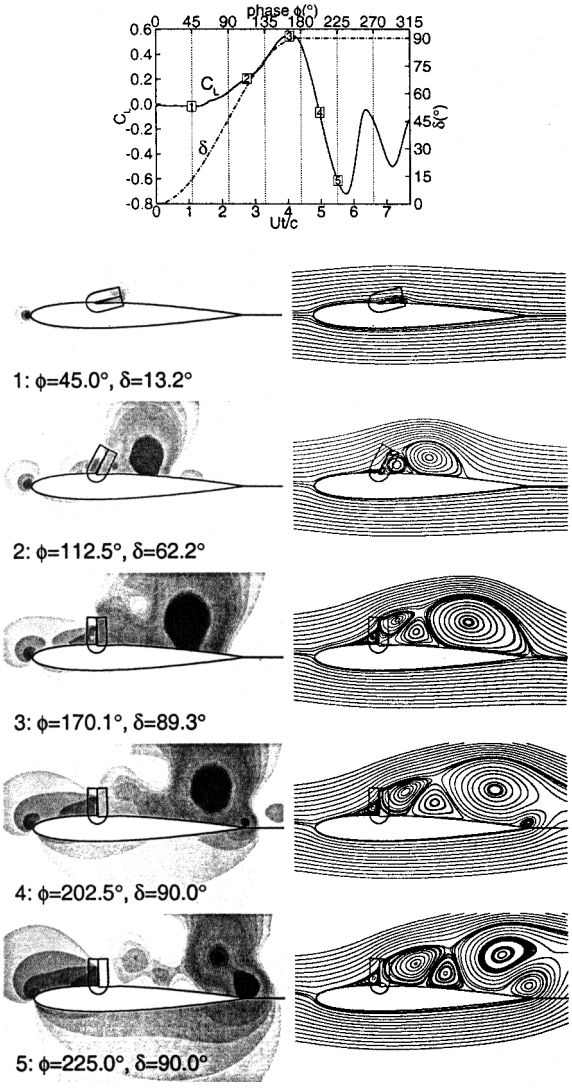

Fig. 9 Flow development with spoiler deployment ($\omega = 620$ deg/s, spoiler location = $0.3c$, hinge gap = 0%): left pressure distributions and right streamlines.

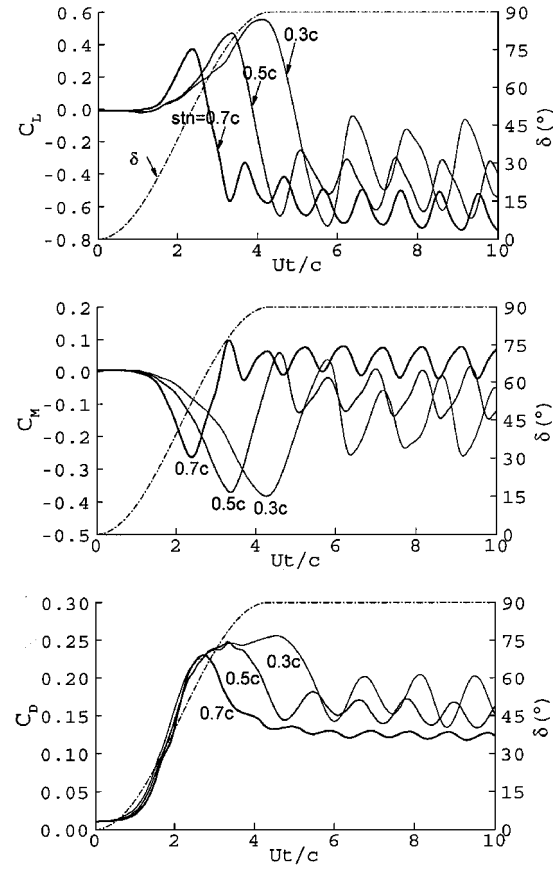

Fig. 10 Transient aerodynamic response depending on the spoiler location (stn) (ω = 620 deg/s, hinge gap = 0%).

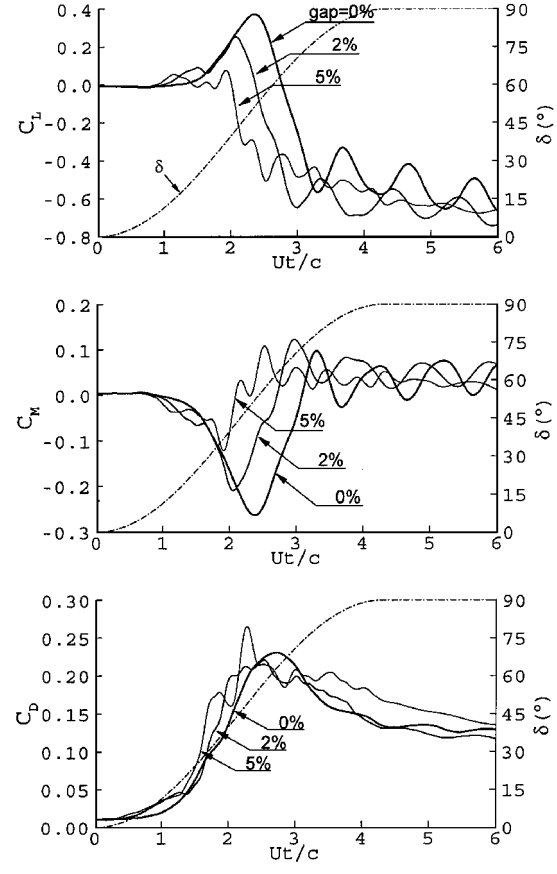

Fig. 11 Transient aerodynamic response depending on the size of the hinge gap (ω = 620 deg/s, spoiler location = $0.7c$).

the three turbulence models are different, the frequency is almost identical for all three models. Note that the Baldwin–Lomax model gives the highest oscillation amplitude, and the SST $k-\omega$ model gives the lowest. The mean value of oscillation is higher than the experimental value for all of the three turbulence models considered here.

The pitching moment coefficient shown in Fig. 6 suggests a considerable amount of initial nose-down (negative) moment, which is much higher than the mean value of the quasi-steady oscillatory state after full deployment of the spoiler. For the drag coefficient, comparisons with the measured data are, in general, favorable, except in the initial stage where the peak values are overpredicted.

The field pressures and the instantaneous streamlines calculated using the SST $k-\omega$ model are shown in Fig. 7. With the rapid deployment of the spoiler, a starting vortex with strong suction pressure is formed behind the spoiler. Most of its effect, however, is canceled by the local positive pressure buildup immediately upstream of the spoiler and by the pressure recovered downstream of the bubble. It attributes to the initial sustaining of lift observed in the lift curves (indicated by the number 1) of Fig. 7. With the spoiler angle further increased, the adverse lift increases to a maximum where the vortex bubble extends to the trailing edge of the airfoil: See the case when the phase angle is $\phi = 98$ deg in Fig. 7. This phenomenon is consistent with Mabey's observation[4]: The reattachment point of the bubble reaches just the trailing edge in the time delay t_a. Following the maximum adverse lift, a new vortex started from the trailing edge of the airfoil grows rapidly and interacts with the spoiler vortex as observed in the case $\phi = 112.5$ deg in Fig. 7.

Effect of the Spoiler Location

Based on the earlier flight tests at low speeds, Mabey suggested that larger adverse lift could be attained by moving the spoiler toward the leading edge of the airfoil.[4] To investigate the details of this phenomenon, two more spoiler locations, at $0.5c$ and $0.3c$, were simulated.

The pressure map and the instantaneous streamlines are plotted in Fig. 8 for the spoiler location $0.5c$ and for $0.3c$ in Fig. 9. From Figs. 8 and 9 it is evident that the more upstream the spoiler is located, the larger are the size and the strength of the vortex bubbles triggering the higher adverse effects. The aerodynamic coefficients in Fig. 10 show that higher peak values and larger time delay are obtained for the spoiler located at $0.3c$ near the leading edge. As seen, for the spoiler at $0.3c$, the quasi-steady oscillation after full deployment of the spoiler has a higher amplitude and increased period.

Effect of the Hinge Gap

The hinge gap (see Fig. 2) is used to reduce the initial adverse effects of the spoiler. Following the experiment made by Yeung et al.[5] again, we investigated three cases representing three hinge gaps: 0, 2, and 5% of the airfoil chord length with the spoiler location fixed at $0.7c$.

The lift coefficient in Fig. 11 shows that the adverse lift and its time delay are significantly decreased as the width of the hinge gap is increased. This tendency is in agreement with the experimental findings. The quasi-steady oscillation after the peak value is reached also decreases with the larger hinge gap. Note that the oscillation becomes almost flat with the 5% hinge gap. Similar trends are also evident with the curves representing the variation drag and pitching moment coefficients. Figure 11 indicates that the adverse effect, time delay, and oscillation are all reduced by the use of a large hinge gap.

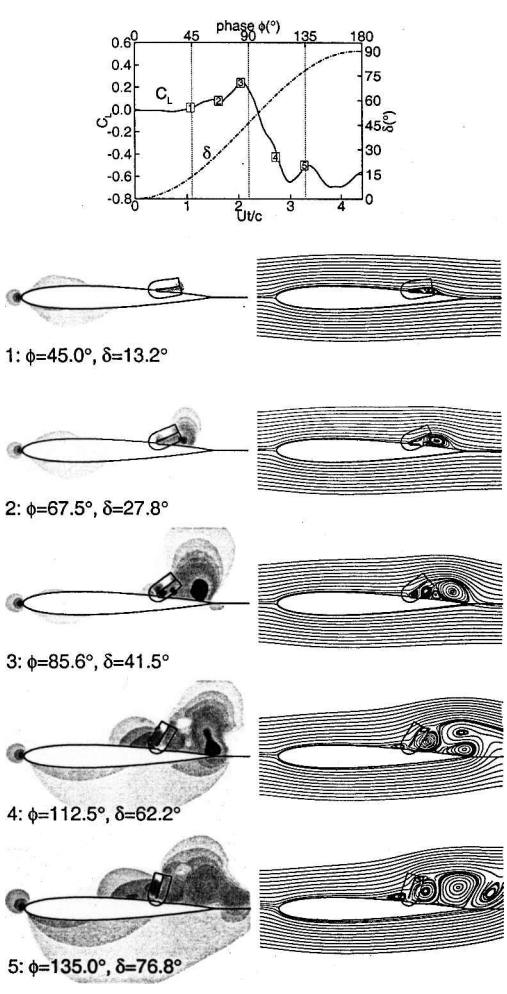

Fig. 12 Flow development with spoiler deployment (ω = 620 deg/s, spoiler location = 0.7c, hinge gap = 2%): left pressure distributions and right streamlines.

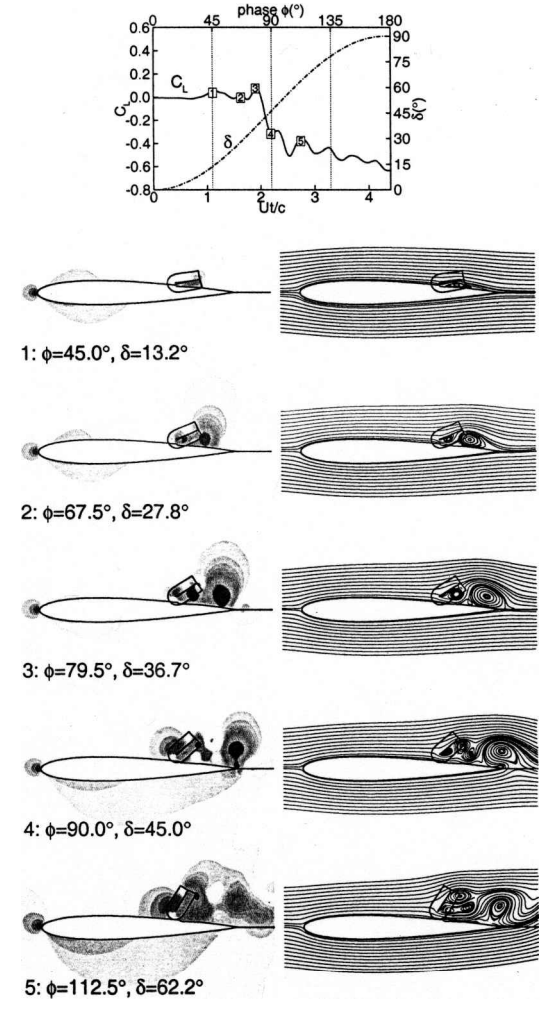

Fig. 13 Flow development with spoiler deployment (ω = 620 deg/s, spoiler location = 0.7c, hinge gap = 5%): left pressure distributions and right streamlines.

The hinge gap can be increased by extending the arm of rotation of the spoiler (see Fig. 2). Comparing Figs. 12 and 13 plotted for the spoiler location at $0.7c$, we observe that the spoiler tip vortex due to the sudden deployment of the spoiler is reduced in size by increasing the hinge gap from 2 to 5%: Compare the maximum adverse lifts at the instant labeled 3. It is due to interaction with the new vortex generated by the base venting of the spoiler. This base vortex has a sense of rotation that is in a direction opposite to that of the spoiler vortex thereby canceling its influence. From Figs. 12 and 13 one can concluded that the base-vented flow through the hinge gap increases the downstream convection velocity of the spoiler vortex. This conclusion is supported by the reduced time delay seen in Fig. 11.

Conclusion

Among the three turbulence models utilized, the SST k–ω model gave the best agreement with the experimental data. The overset grid with the DDDL approach has contributed to the successful computation of the rapidly deploying spoiler with base venting through the hinge gap. The calculated aerodynamic coefficients have shown that the transient adverse effects are reasonably predicted and are in agreement with the existing experimental data. The maximum adverse lift is obtained when the reattachment point of the separation bubble due to the deployed spoiler just reaches the trailing edge of the airfoil. As the spoiler location is moved forward along the chord, the adverse lift and its time delay are more pronounced. The effect of the hinge gap is to reduce the transient behavior of the aerodynamic coefficients. Results of this study should be useful to the designers of a spoiler-based active flow control system, as well as to the developers of a feedback control system for the spoiler.

References

[1]ESDU Aerodynamic Committee, "Controls and Flaps," *ESDU Engineering Science Data*, Vol. 5, No. 90030, ESDU International, 1992, pp. 4–8.

[2]Mabey, D. G., "A Review of Some Recent Research on Time-Dependent Aerodynamics," *Aeronautical Journal*, No. 1099, 1984, pp. 23–37.

[3]Consigny, H., Gravelle, A., and Molinaro, R., "Aerodynamic Characteristics of a Two-Dimensional Moving Spoiler in Subsonic and Transonic Flow," *Journal of Aircraft*, Vol. 21, No. 9, 1984, pp. 687–693.

[4]Mabey, D. G., "On the Prospects for Increasing Dynamic Lift," *Aeronautical Journal*, Vol. 92, No. 1583, 1988, pp. 95–106.

[5]Yeung, W. W. H., Xu, C., and Gu, W., "Reduction of Transient Adverse Effects of Spoilers," *Journal of Aircraft*, Vol. 34, No. 4, 1997, pp. 479–484.

[6]Xu, C., and Yeung, W. W. H., "Unsteady Aerodynamic Characteristics of Airfoil with Moving Spoilers," *Journal of Aircraft*, Vol. 36, No. 3, 1999, pp. 530–540.

[7]Choi, S. W., and Chang, K. S., "Navier–Stokes Computation of a Rapidly Deploying Spoiler," *Journal of Aircraft*, Vol. 37, No. 3, 2000, pp. 655–661.

[8]Baldwin, B., and Lomax, H., "Thin Layer Approximation and Algebraic Model for Separated Turbulent Flows," AIAA Paper 78-257, Jan. 1978.

[9]Pulliam, T. H., "Time Accuracy and the Use of Implicit Method," AIAA Paper 93-3360, July 1993.

[10]Ok, H., "Development of the Incompressible Navier–Stokes Solver and Its Application to the Calculation of Separated Flow," Ph.D. Dissertation, Aeronautics and Astronautics Dept., Univ. of Washington, Seattle, WA, June 1993.

[11]Venkatakrishnan, V., "On the Accuracy of Limiters and Convergence to Steady-State Solutions," AIAA Paper 93-0880, Jan. 1993.

[12]Degani, D., Schiff, L. B., and Levy, Y., "Numerical Prediction of Subsonic Turbulent Flows over Slender Bodies at High Incidence," *AIAA Journal*, Vol. 29, No. 12, 1991, pp. 2054–2061.

[13]Sedaghat, A., Ackroyd, J. A. D., and Wood, N. J., "Turbulence Modelling for Supercritical Flows Including Examples with Passive Shock Control," *Aeronautical Journal*, No. 2409, 1999, pp. 113–125.

[14]Ekaterinaris, J. A., and Mentor, F. R., "Computation of Oscillating Airfoil Flows with One- and Two-Equation Turbulence Models," *AIAA Journal*, Vol. 32, No. 12, 1994, pp. 2359–2365.

[15]Mentor, F. R., "Two-Equation Eddy-Viscosity Turbulence Models for Engineering Applications," *AIAA Journal*, Vol. 32, No. 8, 1994, pp. 1598–1605.

[16]Cook, P. H., McDonald, M. A., and Firmin, M. C. P., "Aerofoil RAE 2822—Pressure Distributions, and Boundary Layer and Wake Measurements," AGARD AR 138, A6, May 1979.

[17]Ok, H., and Eberhardt, D. S., "Calculation of Flowfield Around an Airfoil with Spoiler," AIAA Paper 93-0527, Jan. 1993.

[18]Kim, J. H., and Rho, O. H., "Numerical Simulation of the Flowfield Around an Airfoil with Stationary or Oscillating Spoiler," *Journal of Aircraft*, Vol. 35, No. 5, 1998, pp. 704–711.